Original Article

Quantitative susceptibility mapping study of deep gray matter iron content in glioma patients

Xinlong Liu[1], Zonggang Hou[1], Qifeng He[1], Hongfang Zhao[1], Shengjun Sun[2,3], Shuyu Hao[1], Jian Xie[1]^

[1]Department of Neurosurgery, Beijing Tiantan Hospital, Capital Medical University, Beijing, China; [2]Department of Neuroradiology, Beijing Neurosurgical Institute, Beijing Tiantan Hospital, Capital Medical University, Beijing, China; [3]Department of Radiology, Beijing Tiantan Hospital, Capital Medical University, Beijing, China

Contributions: (I) Conception and design: X Liu, J Xie; (II) Administrative support: J Xie, S Hao, S Sun; (III) Provision of study materials or patients: J Xie, S Sun; (IV) Collection and assembly of data: X Liu, Z Hou, Q He, H Zhao; (V) Data analysis and interpretation: X Liu, J Xie; (VI) Manuscript writing: All authors; (VII) Final approval of manuscript: All authors.

Correspondence to: Jian Xie, MD; Shuyu Hao, MD. Department of Neurosurgery, Beijing Tiantan Hospital, Capital Medical University, No. 119 of South 4th Ring Road, Fengtai District, Beijing 100070, China. Email: xiejian0630@126.com; Shuyuhao@mail.ccmu.edu.cn.

Background: Iron is associated with the pathophysiology of gliomas. The measurement of brain iron levels plays a vital role in defining the pathophysiologic changes caused by gliomas. This study aimed to analyze the effect of gliomas with different histopathology and molecular characteristics on deep gray matter (DGM) iron content and the relationship between DGM iron content and cognition in glioma patients (PT).

Methods: In this retrospective study, we included 81 PT, categorized according to different histopathology and molecular characteristics, and 30 age- and gender-matched healthy controls (HC). Brain quantitative susceptibility mapping (QSM) maps were computed from three-dimensional (3D) multi-echo gradient-echo data using Laplacian-based phase unwrapping, a variational sharpening (V-SHARP) background field correction and the streaking artifacts reduction (STAR)-QSM method. ITK-SNAP was used to measure the susceptibility values reflecting the iron content in the regions of interest. Differences in DGM magnetic susceptibility between groups were compared. Pearson's correlation analysis assessed the relationship between DGM magnetic susceptibility and Montreal Cognitive Assessment (MoCA).

Results: Compared to HC, PT showed higher DGM magnetic susceptibility. QSM analysis exhibited higher DGM magnetic susceptibility in high-grade gliomas (HGG) than low-grade gliomas (LGG). Isocitrate dehydrogenase (IDH) wild-type gliomas showed higher magnetic susceptibility than IDH mutant-type in the putamen [IDH mutant-type: interquartile range (IQR), 0.052, 0.019 ppm *vs.* IDH wild-type: IQR, 0.062, 0.015 ppm, P=0.015]. A higher Ki-67 index also correlated with higher magnetic susceptibility in the putamen (high Ki-67 index group: IQR, 0.063, 0.019 ppm *vs.* low Ki-67 index group: IQR, 0.052, 0.016 ppm, P=0.005). The PT group had significantly lower MoCA scores than the HC group (patients group *vs.* HC group: 22.30±4.92 *vs.* 24.70±2.20, P=0.021). There was a negative correlation between MoCA scores and DGM magnetic susceptibility.

Conclusions: The DGM iron content, as measured by QSM, was higher in PT than in HC and correlated with tumor grade. Cognitive decline is associated with increased DGM iron content in PT. The DGM iron content could be a potential biomarker in glioma differentiation and prognosis.

Keywords: Glioma; quantitative susceptibility mapping (QSM); deep gray matter (DGM); iron; cognition

^ ORCID: 0000-0001-9091-863X.

Submitted Nov 30, 2024. Accepted for publication Mar 12, 2025. Published online Apr 28, 2025.
doi: 10.21037/qims-2024-2704
View this article at: https://dx.doi.org/10.21037/qims-2024-2704

Introduction

Gliomas are the most common primary malignant intracranial tumors in adults and the leading cause of death from primary brain tumors (1-3). According to the 2021 World Health Organization (WHO) classification of central nervous system (CNS) tumors, gliomas are categorized into grades 1–4, ranging from low to high malignancy (2). High-grade gliomas (HGG, grade 3–4) typically exhibit higher mortality rates and shorter survival periods compared to low-grade gliomas (LGG, grade 1–2). In recent years, molecular diagnostics have gained increasing importance in glioma assessment, with the identification of molecular characteristics, particularly isocitrate dehydrogenase (IDH), 1p/19q, and O-6-methylguanine DNA methyltransferase (MGMT) promoter methylation status, being crucial for therapeutic decision-making (1,2). As a non-invasive tool, multiparametric magnetic resonance imaging (MRI) has been widely adopted for preoperative diagnostic evaluation of gliomas (4). Some studies have demonstrated the value of diffusion-weighted imaging (DWI), the T2-fluid-attenuated inversion recovery (FLAIR) mismatch sign, and perfusion-weighted imaging (PWI) in identifying IDH status (4-7).

Iron plays a critical role in nerve cell development and is essential for tumor cell growth, acting as a cofactor for many cellular enzymes (8-10). A growing body of research suggests that iron is associated with the pathophysiology of gliomas (11). Glioblastoma (GBM) expresses high levels of transferrin receptor protein 1 (TfR1), thereby acquiring more iron to support aggressive tumor cell growth (11,12). Consequently, measurement of brain iron levels plays a vital role in defining the pathophysiologic changes of gliomas. Quantitative susceptibility mapping (QSM) can be used for this purpose. QSM is an advanced MRI technique capable of distinguishing between paramagnetic substances (iron, hemosiderin) and diamagnetic substances (calcification) (13,14). Compared to susceptibility-weighted imaging (SWI), QSM offers a higher signal-to-noise ratio, is not geometry-dependent, and can quantitatively measure the magnetic susceptibility of brain tissues (13-15). Iron contributes significantly to changes in the magnetic field, and the magnetic susceptibility levels largely reflect the iron levels. Thus, QSM can more accurately measure tissue iron levels to indicate pathological changes in brain tissues (13,16,17). QSM has emerged as a powerful tool for detecting changes in brain iron content (14,15,18). Although QSM is more commonly used in neurodegenerative diseases (e.g., Parkinson's and Alzheimer's disease) to reflect brain iron levels (19,20), its application in brain tumors remains relatively unexplored. Thus, this study focuses on the use of QSM in glioma patients (PT). We hypothesized that the iron required for the growth of glioma cells is not only increased within the tumor region but also deposited in normal brain regions, such as the iron-rich deep gray matter (DGM) regions. A previous study reported that the quantity of iron in the DGM was well correlated with the magnetic susceptibility of the tissue (21).

Therefore, in this study, we included a group of PT and a group of healthy controls (HC) matched for age and gender to investigate the effect of gliomas with different histopathology and molecular characteristics on DGM iron content. Moreover, we also investigate the relationship between DGM iron content and cognition in PT. We present this article in accordance with the STROBE reporting checklist (available at https://qims.amegroups.com/article/view/10.21037/qims-2024-2704/rc).

Methods

Participants

This study retrospectively analyzed patients diagnosed with glioma at the Department of Neurosurgery, Beijing Tiantan Hospital, Capital Medical University between March 2021 and April 2024. All relevant patient information, including age, gender, histopathology, and molecular characteristics, was obtained from hospital records.

The inclusion criteria were as follows: (I) age between 30 and 60 years; (II) histopathological confirmation of glioma; (III) complete clinical data; (IV) preoperative conventional and advanced MRI including QSM; (V) incipient tumor; and (VI) successful QSM reconstruction. The exclusion criteria were as follows: (I) age <30 or >60 years; (II) histopathological confirmation of non-glioma; (III) incomplete clinical data; (IV) recurrent tumor; (V) DGM regions affected by the tumor; and (VI) failure to reconstruct QSM.

Of the 110 patients diagnosed with glioma during

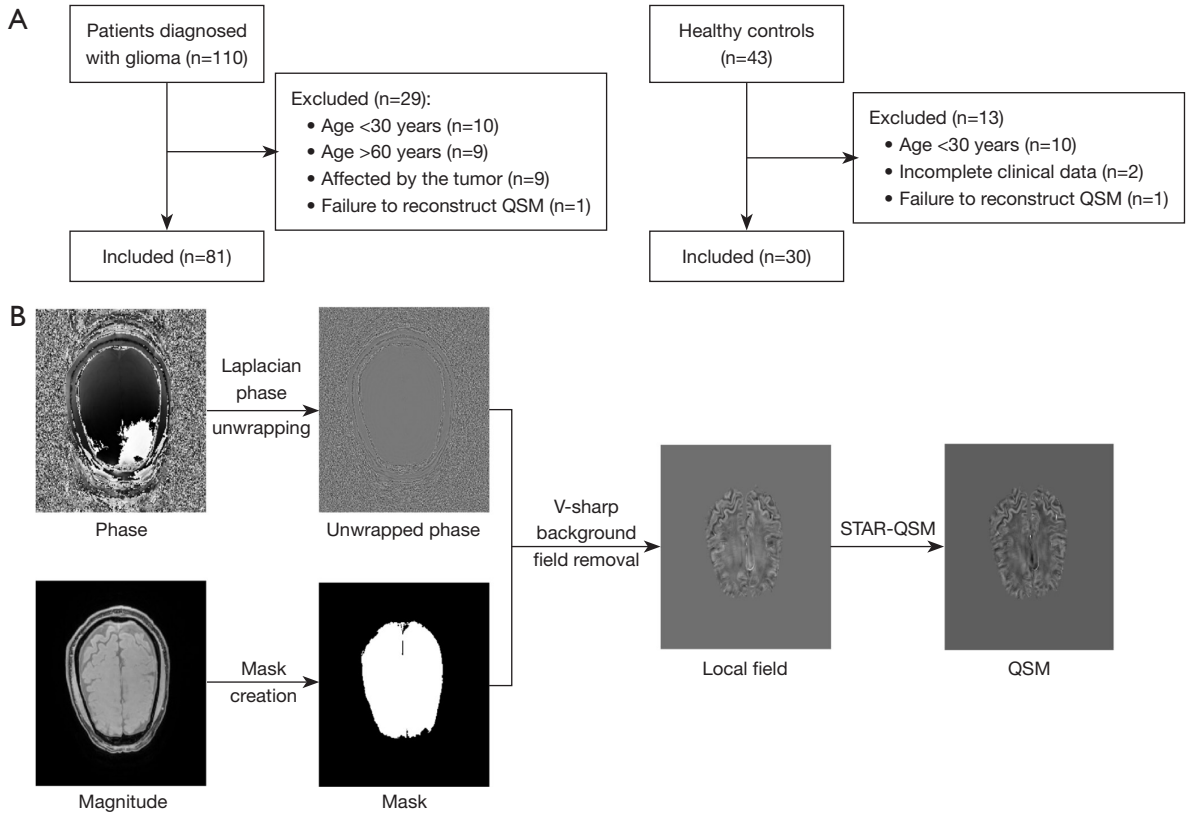

Figure 1 QSM. (A) Flowchart of PT and HC inclusion. (B) Schematic to show quantitative susceptibility mapping processing pipeline used to convert 3D multi-echo gradient-echo images into a susceptibility map using STI suite v3.0. 3D, three-dimensional; HC, healthy controls; PT, glioma patients; QSM, quantitative susceptibility mapping; STAR, streaking artifacts reduction; V-SHARP, variational sharpening.

this period; 81 were included, and 29 were excluded. Additionally, 43 HC were recruited, of whom 30 were included and 13 were excluded. The patient inclusion flowchart is shown in *Figure 1A*. Moreover, 63 participants (33 PT and 30 HC) underwent the cognitive assessment [Montreal Cognitive Assessment (MoCA) Chinese version] (22). To correct for the effect of years of education, 1 point was added for participants with 4 years of education or less on their total MoCA score (but total score ≤30 points). This study used corrected scores.

This study was approved by the Ethics Committee of Beijing Tiantan Hospital, Capital Medical University (No. KY2020–146-02). This study was conducted in accordance with the Declaration of Helsinki and its subsequent amendments. All participants provided written informed consent prior to participating in the study and undergoing MRI procedures.

MRI acquisition

All participants underwent MRI scans using a 3 T MR scanner (MAGNETOM Prisma, Siemens, Erlangen, Germany) at Beijing Tiantan Hospital. The imaging parameters were as follows: repetition time (TR) 40.0 ms; echo time (TE) 7.25 ms, 13.93 ms, 20.61 ms, 27.29 ms; flip angle (FA) 15°; slice thickness 3.0 mm; voxel size 0.8 mm × 0.8 mm × 3.0 mm; echo train length (ETL) 4; pixel spacing 0.764/0.764 mm; field of view (FOV) read 220 mm; FOV phase 90.97%; matrix size 262×288; pixel bandwidth 260 Hz; slices per slab 44; slice oversampling 27.3%; slice resolution 100%; phase resolution 100%; readout resolution 100%; parallel imaging technique; R=2; and 64-channel head/neck coil.

MRI processing

QSM maps were reconstructed from phase and magnitude maps as follows (*Figure 1B*): (I) data loading; (II) parameter setting; (III) mask creation; (IV) phase unwrapping using a Laplacian-based approach; (V) background field removal using variational sharpening (V-SHARP) filtering; and (VI)

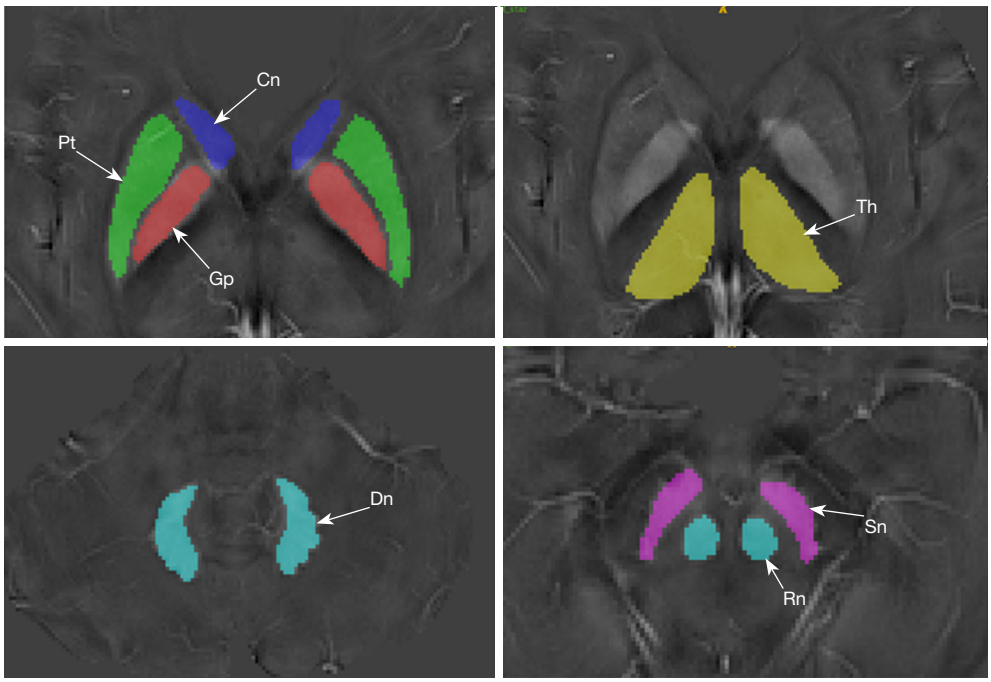

Figure 2 The manually-traced ROIs: Pt, Gp, Cn, Th, Sn, Rn, and cerebellar Dn. Cn, caudate nucleus; Dn, dentate nucleus; Gp, globus pallidus; Pt, putamen; Rn, red nucleus; ROIs, regions of interest; Sn, substantia nigra; Th, thalamus.

field-to-susceptibility inversion using streaking artifacts reduction QSM (STAR-QSM). All steps were performed in MATLAB (R2013b, MathWorks, Natick, MA, USA) using the STI Suite toolbox (https://people.eecs.berkeley.edu/~chunlei.liu/software.html) (23,24).

Image analysis

Brain regions of interest (ROIs) included the putamen (Pt), globus pallidus (Gp), caudate nucleus (Cn), thalamus (Th), substantia nigra (Sn), red nucleus (Rn), and cerebellar dentate nucleus (Dn). These were manually segmented by experienced neuro-radiologists using ITK-SNAP software (*Figure 2*). Segmentation was performed on QSM images due to their superior differentiation between surrounding tissue and ROIs (25). QSM values for each ROI were averaged across bilateral multiple axial slices.

Statistical analysis

All statistical analyses were performed using SPSS 27.0 (IBM Corp., Armonk, NY, USA). Demographic and clinical characteristics were analyzed between groups using Chi-squared or two independent samples *t*-test. Non-parametric tests were used for non-normally distributed data. Age was used as a covariate, and analysis of covariance (ANCOVA) was used to compare cognitive scores (MoCA), magnetic susceptibility values for specific ROIs between PT and HC, and DGM magnetic susceptibility values between different grades of gliomas. When $P<0.05$, *post-hoc* test of least significant difference (LSD) was used for pairwise comparisons. Pearson's correlation analysis assessed the relationship between DGM magnetic susceptibility and MoCA. Receiver operating characteristic (ROC) curves evaluated diagnostic performance of significant indicators, calculating area under the curve (AUC), 95% confidence interval (CI), specificity, and sensitivity. Normality and variance homogeneity were assessed using Shapiro-Wilk and Levene tests, respectively. A P value <0.05 was considered statistically significant.

Results

Demographic and clinical characteristics

Table 1 summarizes the basic information of 81 PT and 30 HC. The mean and median ages were 45.43 and 46.50 years in the HC group, and 44.26 and 43.00 years in the PT group, respectively, with no significant difference between groups (P=0.463). The HC group comprised 15 males and 15

Table 1 The clinical characteristics of healthy controls and glioma patients

Characteristics	HC	PT	P value
Number	30	81	
Age (years)			0.463[&]
Mean	45.43	44.26	
Median	46.50	43.00	
Gender	30	81	0.523[#]
Male	15	46	
Female	15	35	
IDH	NA	81	NA
Mutant-type		46	
Wild-type		35	
1p/19q	NA	81	NA
Co-deletion		22	
Non-codeletion		59	
MGMT[$]	NA	80	NA
Methylation		50	
Unmethylated		30	
TERT	NA	81	NA
Mutant-type		45	
Wild-type		36	
Ki-67 index	NA	81	NA
≥10% (high Ki-67 index group)		35	
<10% (low Ki-67 index group)		46	
CNS WHO classification	NA	81	NA
2		28	
3		27	
4		26	
Number of cognitive assessments	30	33	
Gender (male)	15	19	0.547[#]
Age (years)[§]	45.43±7.93	46.67±8.26	0.549[†]
Education (years)[§]	10.83±3.10	10.64±4.50	0.842[†]
MoCA[§]	24.70±2.20	22.30±4.92	0.021[‡]

[&], Mann-Whitney tests; [#], Chi-squared test; [$], one patient's MGMT information was lost; [†], two independent samples *t*-test; [‡], analysis of covariance, age as a covariate; [§], values are given in mean ± standard deviation. CNS, central nervous system; HC, healthy controls; IDH, isocitrate dehydrogenase; MGMT, O-6-methylguanine DNA methyltransferase; MoCA, Montreal Cognitive Assessment; NA, not applicable; PT, glioma patients; TERT, telomerase reverse transcriptase; WHO, World Health Organization.

females, whereas the PT group had 46 males and 35 females, showing no significant gender difference (P=0.523). In the PT group, there were 46 IDH mutant-type and 35 wild-type cases, 22 1p/19q co-deletion and 59 non-codeletion cases, 50 MGMT promoter methylation and 30 non-methylation cases, 45 TERT mutant-type and 36 wild-type cases, and 35 cases with Ki-67 index ≥10% (high Ki-67 index group) and 46 cases <10% (low Ki-67 index group). In terms of cognitive scores,

Table 2 Description of DGM magnetic susceptibility in HC and PT

ROI	HC	PT	P value
Putamen	0.045±0.011	0.058±0.014	<0.001*
Globus pallidus	0.081±0.014	0.093±0.012	<0.001*
Caudate nucleus	0.031±0.006	0.037±0.007	<0.001*
Thalamus	0.013±0.004	0.017±0.004	<0.001*
Substantia nigra	0.079±0.014	0.093±0.018	<0.001*
Red nucleus	0.074±0.014	0.082±0.018	0.016*
Dentate nucleus	0.058±0.014	0.071±0.016	<0.001*

Values are given in mean ± standard deviation (ppm) and retained to three decimal places. The DGM magnetic susceptibility was analyzed by ANCOVA, with age as a covariate. *, statistical significance. ANCOVA, analysis of covariance; DGM, deep gray matter; HC, healthy control group; PT, patient group; ROI, region of interest.

even after controlling for age, MoCA was lower in PT than in HC (P=0.021, PT: 22.30±4.92; HC: 24.70±2.20), but there were no significant differences in age, gender, and years of education between the two groups (P>0.05).

PT versus HC groups

Statistical analysis revealed significantly higher DGM magnetic susceptibility in all PT groups than HC groups, indicating higher DGM iron content in PT than in HC (*Table 2*). ROC analysis showed that the Pt magnetic susceptibility [AUC =0.77 (95% CI: 0.68–0.86)] had a higher diagnostic value in identifying gliomas. The sensitivity, specificity, and cut-off values were 62%, 83%, and 0.052 ppm, respectively. The detailed results for each region are as follows:

(I) Pt: HC: 0.045±0.011 ppm versus PT: 0.058± 0.014 ppm, P<0.001 (*Figure 3A*); ROC analysis: AUC =0.77 (95% CI: 0.68–0.86), sensitivity: 62%, specificity: 83%.

(II) Gp: HC: 0.081±0.014 ppm versus PT: 0.093± 0.012 ppm, P<0.001 (*Figure 3B*); ROC analysis: AUC =0.74 (95% CI: 0.64–0.85), sensitivity: 67%, specificity: 77%.

(III) Cn: HC: 0.031±0.006 ppm versus PT: 0.037± 0.007 ppm, P<0.001 (*Figure 3C*); ROC analysis: AUC =0.77 (95% CI: 0.67–0.86), sensitivity: 70%, specificity: 80%.

(IV) Th: HC: 0.013±0.004 ppm versus PT: 0.017± 0.004 ppm, P<0.001 (*Figure 3D*); ROC analysis: AUC =0.77 (95% CI: 0.67–0.87), sensitivity: 79%, specificity: 70%.

(V) Sn: HC: 0.079±0.014 ppm versus PT: 0.093± 0.018 ppm, P<0.001 (*Figure 3E*); ROC analysis: AUC =0.73 (95% CI: 0.63–0.83), sensitivity: 75%, specificity: 63%.

(VI) Rn: HC: 0.074±0.014 ppm versus PT: 0.082± 0.018 ppm, P=0.016 (*Figure 3F*); ROC analysis: AUC =0.64 (95% CI: 0.53–0.74), sensitivity: 47%, specificity: 83%.

(VII) Dn: HC: 0.058±0.014 ppm versus PT: 0.071± 0.016 ppm, P<0.001 (*Figure 3G*); ROC analysis: AUC =0.73 (95% CI: 0.63–0.83), sensitivity: 65%, specificity: 77%.

Comparison among different grades of gliomas

Overall, HGG demonstrated higher magnetic susceptibility than LGG, but no significant difference was observed between glioma grades 3 and 4. HGG exhibited significantly higher magnetic susceptibility compared to HC, whereas LGG also showed higher values, but the difference was not statistically significant in some regions, such as Sn, Rn, and Dn (*Table 3*, Tables S1-S7 shows the *post-hoc* test of LSD results). The detailed results for each region were as follows:

(I) Pt: HC: 0.045±0.011 ppm, Grade 2: 0.051± 0.011 ppm, Grade 3: 0.061±0.015 ppm, Grade 4: 0.063±0.012 ppm, P<0.001 (*Figure 4A*).

(II) Gp: HC: 0.081±0.014 ppm, Grade 2: 0.092± 0.013 ppm, Grade 3: 0.094±0.011 ppm, Grade 4: 0.094±0.012 ppm, P<0.001 (*Figure 4B*).

(III) Cn: HC: 0.031±0.006 ppm, Grade 2: 0.035± 0.006 ppm, Grade 3: 0.037±0.006 ppm, Grade 4: 0.039±0.007 ppm, P<0.001 (*Figure 4C*).

(IV) Th: HC: 0.013±0.004 ppm, Grade 2: 0.015± 0.003 ppm, Grade 3: 0.018±0.005 ppm, Grade 4:

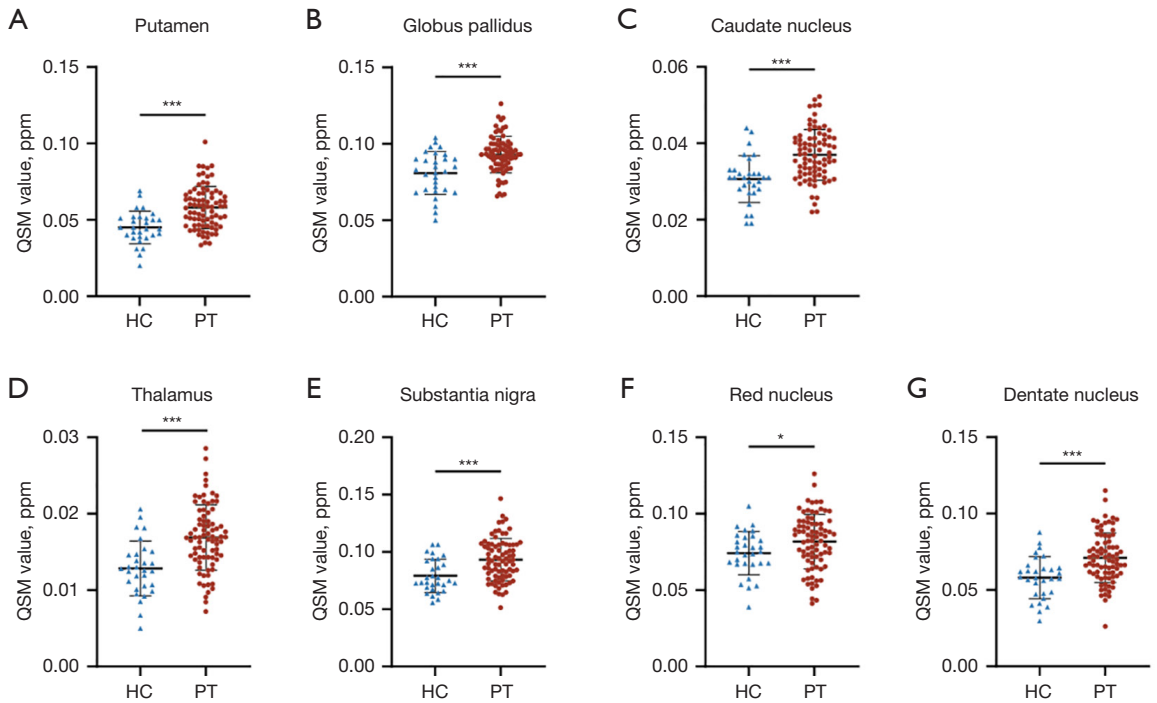

Figure 3 Comparison of magnetic susceptibility between PT and HC in different DGM regions: (A) putamen; (B) globus pallidus; (C) gaudate nucleus; (D) thalamus; (E) substantia nigra; (F) red nucleus; (G) dentate nucleus. *, P<0.05; ***, P<0.001. DGM, deep gray matter; HC, healthy controls; PT, glioma patients; QSM, quantitative susceptibility mapping.

Table 3 Description of DGM magnetic susceptibility in different grades of gliomas

ROI	HC	Grade 2	Grade 3	Grade 4	P value
Putamen	0.045±0.011	0.051±0.011	0.061±0.015	0.063±0.012	<0.001*
Globus pallidus	0.081±0.014	0.092±0.013	0.094±0.011	0.094±0.012	<0.001*
Caudate nucleus	0.031±0.006	0.035±0.006	0.037±0.006	0.039±0.007	<0.001*
Thalamus	0.013±0.004	0.015±0.003	0.018±0.005	0.018±0.004	<0.001*
Substantia nigra	0.079±0.014	0.086±0.014	0.095±0.017	0.099±0.021	<0.001*
Red nucleus	0.074±0.014	0.073±0.016	0.087±0.018	0.086±0.016	0.002*
Dentate nucleus	0.058±0.014	0.065±0.017	0.076±0.015	0.072±0.015	<0.001*

Values are given in mean ± standard deviation (ppm) and retained to three decimal places. The DGM magnetic susceptibility was analyzed by ANCOVA, with age as a covariate. The results of pairwise comparison between different grades after multiple comparisons were presented in Tables S1-S7. *, statistical significance. ANCOVA, analysis of covariance; DGM, deep gray matter; HC, healthy control group; ROI, region of interest.

0.018±0.004 ppm, P<0.001 (*Figure 4D*).

(V) Sn: HC: 0.079±0.014 ppm, Grade 2: 0.086±0.014 ppm, Grade 3: 0.095±0.017 ppm, Grade 4: 0.099±0.021 ppm, P<0.001 (*Figure 4E*).

(VI) Rn: HC: 0.074±0.014 ppm, Grade 2: 0.073±0.016 ppm, Grade 3: 0.087±0.018 ppm, Grade 4: 0.086±0.016 ppm, P=0.002 (*Figure 4F*).

(VII) Dn: HC: 0.058±0.014 ppm, Grade 2: 0.065±0.017 ppm, Grade 3: 0.076±0.015 ppm, Grade 4: 0.072±0.015 ppm, P<0.001 (*Figure 4G*).

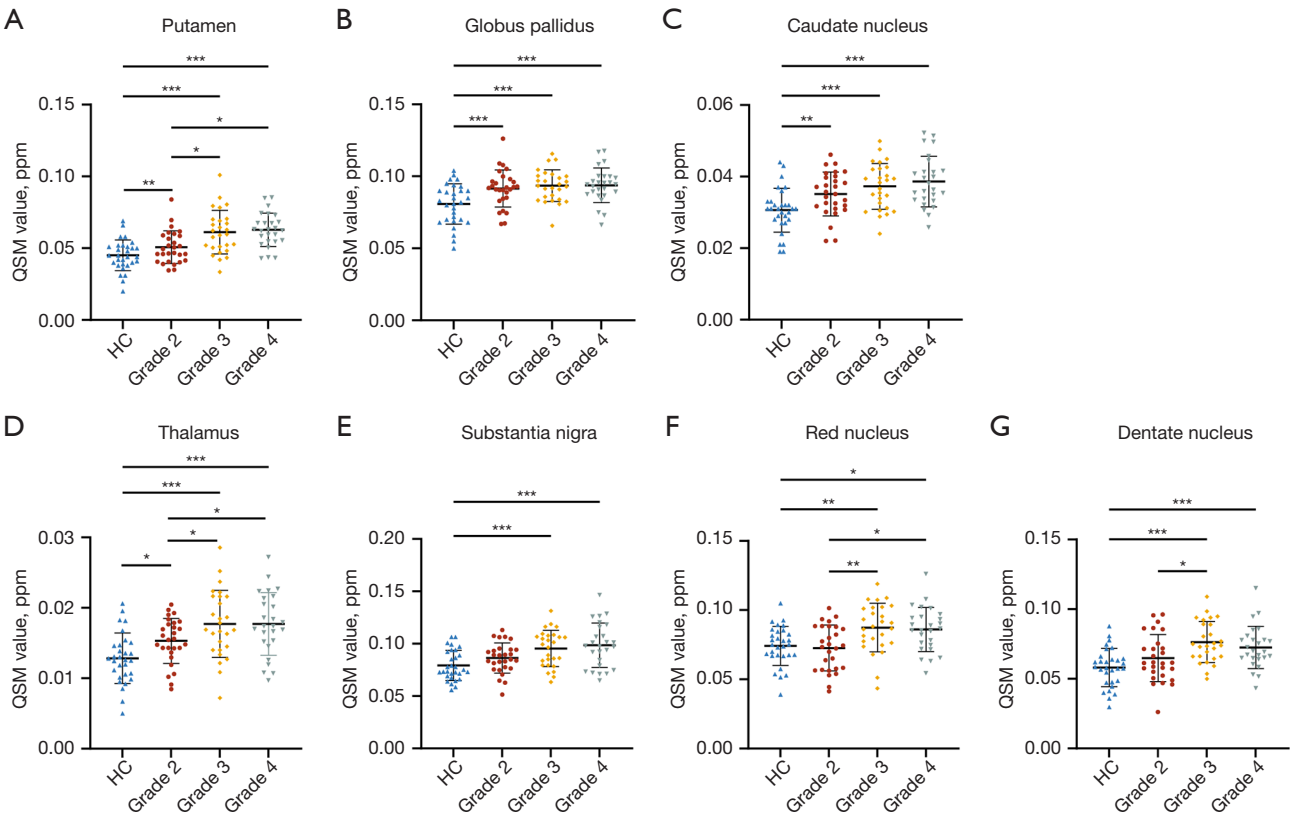

Figure 4 Comparison of magnetic susceptibility among different grades of gliomas in different DGM regions: (A) putamen; (B) globus pallidus; (C) gaudate nucleus; (D) thalamus; (E) substantia nigra; (F) red nucleus; (G) dentate nucleus. *, P<0.05; **, P<0.01; ***, P<0.001. Grade 2: patients with grade 2 gliomas; Grade 3: patients with grade 3 gliomas; Grade 4: patients with grade 4 gliomas. DGM, deep gray matter; HC, healthy controls; QSM, quantitative susceptibility mapping.

Molecular characteristics

Pt magnetic susceptibility significantly differed in identifying IDH status, with IDH wild-type showing higher values than IDH mutant-type [IDH mutant-type: interquartile range (IQR), 0.052, 0.019 ppm *vs.* IDH wild-type: IQR, 0.062, 0.015 ppm, P=0.015, *Table 4*, *Figure 5A*]. ROC analysis: AUC =0.66 (95% CI: 0.54–0.78), sensitivity: 77%, specificity: 54%.

Regarding Ki-67 index, the high Ki-67 index group generally showed higher magnetic susceptibility than the low Ki-67 index group, except in the Dn (*Table 4*). This difference was more pronounced in the Pt (high Ki-67 index group: IQR, 0.063, 0.019 ppm *vs.* low Ki-67 index group: IQR, 0.052, 0.016 ppm, P=0.005, *Table 4*, *Figure 5B*). ROC analysis for Pt: AUC =0.68 (95% CI: 0.56–0.80), sensitivity: 57%, specificity: 80%.

DGM magnetic susceptibility showed limited value in identifying 1p/19q co-deletion status, MGMT promoter methylation status, and TERT status.

Pearson's correlation analysis

When only PT were considered, there was no statistical difference, although susceptibility of each subcortical structure was negatively correlated with cognitive scores (*Table 5*). When all the participants were considered, there was a significantly negative correlation between MoCA scores and susceptibility in the Pt (r=–0.364, P=0.003), Gp (r=–0.263, P=0.037), Cn (r=–0.292, P=0.020), Sn (r=–0.353, P=0.004), and Dn (r=–0.306, P=0.015) (*Table 5*).

Discussion

In this study, we quantitatively measured DGM magnetic susceptibility using QSM to reflect tissue iron content.

Table 4 Description of DGM magnetic susceptibility in IDH and Ki-67 index

ROI	IDH			Ki-67 index		
	Mutant-type	Wild-type	P value	≥10%[$]	<10%[&]	P value
Putamen[§]	0.052, 0.019[#]	0.062, 0.015[#]	0.015*	0.063, 0.019[#]	0.052, 0.016[#]	0.005*
Globus pallidus	0.093±0.013	0.093±0.011	0.828	0.094±0.012	0.092±0.012	0.447
Caudate nucleus	0.036±0.006	0.038±0.007	0.232	0.038±0.006	0.036±0.007	0.322
Thalamus	0.016±0.004	0.017±0.004	0.324	0.017±0.004	0.017±0.005	0.684
Substantia nigra	0.092±0.017	0.095±0.019	0.367	0.097±0.019	0.091±0.017	0.132
Red nucleus	0.080±0.018	0.085±0.018	0.214	0.085±0.018	0.079±0.018	0.146
Dentate nucleus	0.070±0.017	0.072±0.015	0.560	0.070±0.012	0.072±0.019	0.625

Values are given in mean ± standard deviation (ppm) and retained to three decimal places. [§], the putamen magnetic susceptibility was analyzed by Mann-Whitney tests. The other DGM regions magnetic susceptibility was analyzed by two-independent-sample *t*-tests; [#], values are presented as median and interquartile range due to non-normal distribution; [$], high Ki-67 index group; [&], low Ki-67 index group; *, statistical significance. DGM, deep gray matter; IDH, isocitrate dehydrogenase; ROI, region of interest.

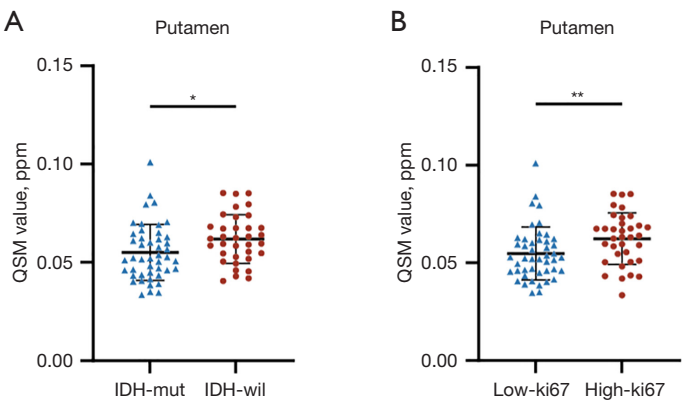

Figure 5 Comparison of magnetic susceptibility in different molecular characteristics. (A) IDH; (B) Ki-67. *, P<0.05; **, P<0.01. IDH-mut: IDH mutant-type glioma patient group; IDH-wil: IDH wild-type glioma patient group; Low-ki67: low Ki-67 index group; High-ki67: high Ki-67 index group. IDH, isocitrate dehydrogenase; QSM, quantitative susceptibility mapping.

Table 5 Pearson's correlation analysis

ROI	Gliomas		The entire participants	
	r	P value	r	P value
Putamen	–0.257	0.148	–0.364	0.003*
Globus pallidus	–0.150	0.404	–0.263	0.037*
Caudate nucleus	–0.224	0.210	–0.292	0.020*
Thalamus	–0.030	0.868	–0.150	0.242
Substantia nigra	–0.254	0.154	–0.353	0.004*
Red nucleus	–0.100	0.578	–0.200	0.117
Dentate nucleus	–0.216	0.226	–0.306	0.015*

Pearson's correlation analysis assessed the simple univariable relationship between DGM magnetic susceptibility and cognitive scores. *, statistical significance. DGM, deep gray matter; ROI, region of interest.

Our results demonstrated that DGM iron content in PT was higher than that in HC, consistent with previous studies that the T2 shortening in the basal ganglia and Th of brain tumor patients compared to HC (26). The T2 shortening was suggestive of an increased iron content. This phenomenon has also been observed in neurodegenerative diseases (23,27,28). Patients with neurodegenerative diseases are often accompanied by cognitive decline, which has been shown to be associated with increased iron content in DGM (29-31). Cognitive decline has also been observed in PT (32). Our results indicate that PT have significantly lower MoCA scores than HC. Moreover, Pearson's correlation analysis showed a significantly negative correlation between iron content and cognitive ability in the Pt, Gp, Cn, Sn, and Dn, which may be related to neurodegenerative pathology due to increased iron content in DGM in PT. One of the poor prognostic factors in GBMs is the compromised neurocognitive status at the initial stage, this also predicts that higher DGM iron content might be associated with a poorer prognosis.

Furthermore, we found that the increase in iron content was more pronounced in HGG than in LGG. However, the difference in iron content between glioma grades 3 and 4 was insignificant. Although DGM iron content in LGG was higher than in HC, the difference was not pronounced in certain regions, such as the Sn, Rn, and Dn. These results suggest that DGM iron content increases with glioma grade. This is consistent with the previous findings of Reith *et al.* that the basal ganglia iron content increased with glioma severity (33).

The potential role of DGM iron content in the differentiation of gliomas warrants consideration. It is crucial to note that oncologic and non-oncologic diseases necessitate distinct treatment strategies. Although biopsy remains the gold standard for diagnosis, it is an invasive procedure associated with risks and potential tissue sampling errors (34). MRI, as a non-invasive alternative, offers valuable insights for glioma evaluation (35). When differentiation between gliomas and other non-oncologic diseases proves challenging, QSM can be used in combination with other diagnostic tools to help in the differential diagnosis of glioma. The diagnostic efficacy of the Pt was the best according to the results of the ROC analysis, suggesting its potential as a biomarker for differentiating gliomas from non-oncologic conditions. It is unclear whether this phenomenon of increased iron content in DGM regions occurs in other brain tumors; further research is needed.

Our findings indicate that DGM iron content has limited value in identifying molecular characteristics of gliomas. However, Pt iron content showed some potential in identifying IDH status. It is important to note that there is significant overlap between IDH mutation status and glioma grading according to the 2021 WHO classification of CNS tumors (36). Therefore, the role of Pt iron content in identifying IDH mutation status requires further investigation. Nevertheless, our results demonstrate that Pt iron content is significantly correlated with glioma grades, suggesting that the Pt may reflect more tumor severity than other DGM regions. This hypothesis is supported by previous studies on type 2 diabetes patients (37) and amyotrophic lateral sclerosis (ALS) (23), which found that Pt iron content increased more significantly compared to other DGM regions.

The most important influence on DGM iron content appears to be tumor grade, further confirmed by the Ki-67 index. We observed that higher Ki-67 index correlated with higher DGM iron content in PT, with higher Ki-67 index representing increased tumor proliferative activity and more severe tumors (38,39). The observed elevation in DGM iron content among PT may be attributed to the increased iron requirements of rapidly proliferating tumor cells. Excessive iron can induce oxidative stress; as a protective mechanism, ferritin molecules sequester and store ferrous ions, potentially resulting in heightened deposition of iron compounds within DGM regions (26). It has been well known that some anatomical regions, such as the Gp and Sn, are more prone to iron accumulation than others (40), but the mechanism of this regional heterogeneity remains unknown. Some studies have shown that GBM upregulates iron transporter transferrin (41) and transferrin receptor (11,12,42), thereby increasing iron uptake.

Disruption of the blood-brain barrier (BBB) may be related to DGM iron deposition. The BBB is composed of a highly selective semipermeable border formed by capillary endothelial cells, astrocytic end-feet, and pericytes embedded in the basement membrane that prevents solutes in the circulating blood from non-selectively crossing into the brain (43,44). When the BBB is disrupted by gliomas, low-molecular-weight molecules in the blood (e.g., ferrous and ferric ions) are more readily transported to the brain. Moreover, the disruption of the BBB leads to a reduced clearance function, which will further exacerbate the increase in brain iron levels (44-46).

Our study innovatively used QSM to quantitatively compare DGM iron content between PT and HC,

and to explore its application in identifying molecular characteristics of gliomas. However, our study has limitations. Firstly, the sample size is relatively small and lacking in grade 1 PT. Future investigations should aim to expand the cohort to include a broader spectrum of glioma grades and a larger number of cases. Secondly, ROI-based analyses may be subject to selection bias due to subjective differences among investigators. To mitigate this, we involved experienced neuroradiologists in segmenting and correcting ROIs. Thirdly, the relatively low spatial resolution of the acquired image data may have led to an underestimation of susceptibility, but the same imaging parameters were used for all participants and therefore did not significantly affect the results. Lastly, the lack of postmortem measurements of DGM iron content in our study population prevents definitive confirmation that increased magnetic susceptibility values were due to increased iron content. However, previous studies have shown close agreement between postmortem measurements of brain iron concentrations and QSM observations (47-49).

Although this study demonstrates increased DGM iron content in PT, this finding represents a preliminary conclusion. The specific patterns and mechanisms of iron deposition in these regions remain to be elucidated and should be the focus of future investigations. Furthermore, the potential for gliomas to induce iron deposition in the cerebral cortex is an intriguing question that warrants dedicated exploration. These research results could provide valuable insights into the pathophysiologic changes of gliomas and potentially inform new therapeutic approaches.

Conclusions

QSM effectively quantified subcortical iron content in PT and HC. The DGM iron content, as measured by QSM, was higher in PT than in HC and correlated with tumor grade. Cognitive decline is associated with increased DGM iron content in PT. The DGM iron content could be a potential biomarker in glioma differentiation and prognosis.

Acknowledgments

We would like to express our deepest gratitude to all the participants and their families. We wish to thank the National Natural Science Foundation of China for the financial support to our work.

Footnote

Reporting Checklist: The authors have completed the STROBE reporting checklist. Available at https://qims.amegroups.com/article/view/10.21037/qims-2024-2704/rc

Funding: This work was supported by the National Natural Science Foundation of China (No. 82172028).

Conflicts of Interest: All authors have completed the ICMJE uniform disclosure form (available at https://qims.amegroups.com/article/view/10.21037/qims-2024-2704/coif). J.X. reports that this study was supported by the National Natural Science Foundation of China (No. 82172028). The other authors have no conflicts of interest to declare.

Ethical Statement: The authors are accountable for all aspects of the work in ensuring that questions related to the accuracy or integrity of any part of the work are appropriately investigated and resolved. This study was conducted in accordance with the Declaration of Helsinki and its subsequent amendments and was approved by the Ethics Committee of Beijing Tiantan Hospital, Capital Medical University (No. KY2020–146-02). All participants provided written informed consent prior to participating in the study and undergoing MRI procedures.

References

1. van den Bent MJ, Geurts M, French PJ, Smits M, Capper D, Bromberg JEC, Chang SM. Primary brain tumours in adults. Lancet 2023;402:1564-79.
2. Weller M, Wen PY, Chang SM, Dirven L, Lim M, Monje M, Reifenberger G. Glioma. Nat Rev Dis Primers 2024;10:33.

3. Nicholson JG, Fine HA. Diffuse Glioma Heterogeneity and Its Therapeutic Implications. Cancer Discov 2021;11:575-90.
4. Chu JP, Song YK, Tian YS, Qiu HS, Huang XH, Wang YL, Huang YQ, Zhao J. Diffusion kurtosis imaging in evaluating gliomas: different region of interest selection methods on time efficiency, measurement repeatability, and diagnostic ability. Eur Radiol 2021;31:729-39.
5. Hu LS, Hawkins-Daarud A, Wang L, Li J, Swanson KR. Imaging of intratumoral heterogeneity in high-grade glioma. Cancer Lett 2020;477:97-106.
6. Foltyn M, Nieto Taborda KN, Neuberger U, Brugnara G, Reinhardt A, Stichel D, Heiland S, Herold-Mende C, Unterberg A, Debus J, von Deimling A, Wick W, Bendszus M, Kickingereder P. T2/FLAIR-mismatch sign for noninvasive detection of IDH-mutant 1p/19q non-codeleted gliomas: validity and pathophysiology. Neurooncol Adv 2020;2:vdaa004.
7. Sun Y, Yang Z, Deng K, Geng Y, Hu X, Song Y, Jiang R. Histogram analysis of quantitative susceptibility mapping and apparent diffusion coefficient for identifying isocitrate dehydrogenase genotypes and tumor subtypes of adult-type diffuse gliomas. Quant Imaging Med Surg 2023;13:8681-93.
8. Chen Y, Su S, Dai Y, Zou M, Lin L, Qian L, Zhou Q, Zhang H, Liu M, Zhao J, Yang Z. Quantitative susceptibility mapping reveals brain iron deficiency in children with attention-deficit/hyperactivity disorder: a whole-brain analysis. Eur Radiol 2022;32:3726-33.
9. Bystrom LM, Rivella S. Cancer cells with irons in the fire. Free Radic Biol Med 2015;79:337-42.
10. Torti SV, Torti FM. Iron and cancer: more ore to be mined. Nat Rev Cancer 2013;13:342-55.
11. Legendre C, Garcion E. Iron metabolism: a double-edged sword in the resistance of glioblastoma to therapies. Trends Endocrinol Metab 2015;26:322-31.
12. Voth B, Nagasawa DT, Pelargos PE, Chung LK, Ung N, Gopen Q, Tenn S, Kamei DT, Yang I. Transferrin receptors and glioblastoma multiforme: Current findings and potential for treatment. J Clin Neurosci 2015;22:1071-6.
13. Liu C, Li W, Tong KA, Yeom KW, Kuzminski S. Susceptibility-weighted imaging and quantitative susceptibility mapping in the brain. J Magn Reson Imaging 2015;42:23-41.
14. Haacke EM, Liu S, Buch S, Zheng W, Wu D, Ye Y. Quantitative susceptibility mapping: current status and future directions. Magn Reson Imaging 2015;33:1-25.
15. Yan F, He N, Lin H, Li R. Iron deposition quantification: Applications in the brain and liver. J Magn Reson Imaging 2018;48:301-17.
16. Haacke EM, Cheng NY, House MJ, Liu Q, Neelavalli J, Ogg RJ, Khan A, Ayaz M, Kirsch W, Obenaus A. Imaging iron stores in the brain using magnetic resonance imaging. Magn Reson Imaging 2005;23:1-25.
17. Madden DJ, Merenstein JL. Quantitative susceptibility mapping of brain iron in healthy aging and cognition. Neuroimage 2023;282:120401.
18. Nikparast F, Ganji Z, Danesh Doust M, Faraji R, Zare H. Brain pathological changes during neurodegenerative diseases and their identification methods: How does QSM perform in detecting this process? Insights Imaging 2022;13:74.
19. Guan X, Lancione M, Ayton S, Dusek P, Langkammer C, Zhang M. Neuroimaging of Parkinson's disease by quantitative susceptibility mapping. Neuroimage 2024;289:120547.
20. Ravanfar P, Loi SM, Syeda WT, Van Rheenen TE, Bush AI, Desmond P, Cropley VL, Lane DJR, Opazo CM, Moffat BA, Velakoulis D, Pantelis C. Systematic Review: Quantitative Susceptibility Mapping (QSM) of Brain Iron Profile in Neurodegenerative Diseases. Front Neurosci 2021;15:618435.
21. Sun H, Walsh AJ, Lebel RM, Blevins G, Catz I, Lu JQ, Johnson ES, Emery DJ, Warren KG, Wilman AH. Validation of quantitative susceptibility mapping with Perls' iron staining for subcortical gray matter. Neuroimage 2015;105:486-92.
22. Chen KL, Xu Y, Chu AQ, Ding D, Liang XN, Nasreddine ZS, Dong Q, Hong Z, Zhao QH, Guo QH. Validation of the Chinese Version of Montreal Cognitive Assessment Basic for Screening Mild Cognitive Impairment. J Am Geriatr Soc 2016;64:e285-90.
23. Ghaderi S, Batouli SAH, Mohammadi S, Fatehi F. Iron quantification in basal ganglia using quantitative susceptibility mapping in a patient with ALS: a case report and literature review. Front Neurosci 2023;17:1229082.
24. Li W, Avram AV, Wu B, Xiao X, Liu C. Integrated Laplacian-based phase unwrapping and background phase removal for quantitative susceptibility mapping. NMR Biomed 2014;27:219-27.
25. Persson N, Wu J, Zhang Q, Liu T, Shen J, Bao R, Ni M, Liu T, Wang Y, Spincemaille P. Age and sex related differences in subcortical brain iron concentrations among

healthy adults. Neuroimage 2015;122:385-98.
26. Herynek V, Wagnerová D, Malucelli A, Vymazal J, Sameš M, Hájek M. Alterations in the basal ganglia in patients with brain tumours may be due to excessive iron deposition. Oncol Lett 2015;9:43-6.
27. Sjöström H, Granberg T, Westman E, Svenningsson P. Quantitative susceptibility mapping differentiates between parkinsonian disorders. Parkinsonism Relat Disord 2017;44:51-7.
28. Lee JH, Lee MS. Brain Iron Accumulation in Atypical Parkinsonian Syndromes: in vivo MRI Evidences for Distinctive Patterns. Front Neurol 2019;10:74.
29. Li DTH, Hui ES, Chan Q, Yao N, Chua SE, McAlonan GM, Pang SYY, Ho SL, Mak HKF. Quantitative susceptibility mapping as an indicator of subcortical and limbic iron abnormality in Parkinson's disease with dementia. Neuroimage Clin 2018;20:365-73.
30. Cogswell PM, Wiste HJ, Senjem ML, Gunter JL, Weigand SD, Schwarz CG, Arani A, Therneau TM, Lowe VJ, Knopman DS, Botha H, Graff-Radford J, Jones DT, Kantarci K, Vemuri P, Boeve BF, Mielke MM, Petersen RC, Jack CR Jr. Associations of quantitative susceptibility mapping with Alzheimer's disease clinical and imaging markers. Neuroimage 2021;224:117433.
31. Spence H, McNeil CJ, Waiter GD. The impact of brain iron accumulation on cognition: A systematic review. PLoS One 2020;15:e0240697.
32. Morshed RA, Young JS, Kroliczek AA, Berger MS, Brang D, Hervey-Jumper SL. A Neurosurgeon's Guide to Cognitive Dysfunction in Adult Glioma. Neurosurgery 2021;89:1-10.
33. Reith TP, Prah MA, Choi EJ, Lee J, Wujek R, Al-Gizawiy M, Chitambar CR, Connelly JM, Schmainda KM. Basal Ganglia Iron Content Increases with Glioma Severity Using Quantitative Susceptibility Mapping: A Potential Biomarker of Tumor Severity. Tomography 2022;8:789-97.
34. Khorasani A, Tavakoli MB, Saboori M, Jalilian M. Preliminary study of multiple b-value diffusion-weighted images and T1 post enhancement magnetic resonance imaging images fusion with Laplacian Re-decomposition (LRD) medical fusion algorithm for glioma grading. Eur J Radiol Open 2021;8:100378.
35. Inano R, Oishi N, Kunieda T, Arakawa Y, Kikuchi T, Fukuyama H, Miyamoto S. Visualization of heterogeneity and regional grading of gliomas by multiple features using magnetic resonance-based clustered images. Sci Rep 2016;6:30344.
36. Horbinski C, Berger T, Packer RJ, Wen PY. Clinical implications of the 2021 edition of the WHO classification of central nervous system tumours. Nat Rev Neurol 2022;18:515-29.
37. Li J, Zhang Q, Zhang N, Guo L. Increased Brain Iron Deposition in the Putamen in Patients with Type 2 Diabetes Mellitus Detected by Quantitative Susceptibility Mapping. J Diabetes Res 2020;2020:7242530.
38. Scholzen T, Gerdes J. The Ki-67 protein: from the known and the unknown. J Cell Physiol 2000;182:311-22.
39. Hu X, Miao W, Zou Y, Zhang W, Zhang Y, Liu H. Expression of p53, epidermal growth factor receptor, Ki-67 and O(6)-methylguanine-DNA methyltransferase in human gliomas. Oncol Lett 2013;6:130-4.
40. Rouault TA, Cooperman S. Brain iron metabolism. Semin Pediatr Neurol 2006;13:142-8.
41. Schonberg DL, Miller TE, Wu Q, Flavahan WA, Das NK, Hale JS, Hubert CG, Mack SC, Jarrar AM, Karl RT, Rosager AM, Nixon AM, Tesar PJ, Hamerlik P, Kristensen BW, Horbinski C, Connor JR, Fox PL, Lathia JD, Rich JN. Preferential Iron Trafficking Characterizes Glioblastoma Stem-like Cells. Cancer Cell 2015;28:441-55.
42. Recht L, Torres CO, Smith TW, Raso V, Griffin TW. Transferrin receptor in normal and neoplastic brain tissue: implications for brain-tumor immunotherapy. J Neurosurg 1990;72:941-5.
43. Uchida Y, Kan H, Sakurai K, Horimoto Y, Hayashi E, Iida A, Okamura N, Oishi K, Matsukawa N. APOE ε4 dose associates with increased brain iron and β-amyloid via blood-brain barrier dysfunction. J Neurol Neurosurg Psychiatry 2022. [Epub ahead of print]. doi: 10.1136/jnnp-2021-328519.
44. Uchida Y, Kan H, Sakurai K, Oishi K, Matsukawa N. Contributions of blood-brain barrier imaging to neurovascular unit pathophysiology of Alzheimer's disease and related dementias. Front Aging Neurosci 2023;15:1111448.
45. Uchida Y, Kan H, Furukawa G, Onda K, Sakurai K, Takada K, Matsukawa N, Oishi K. Relationship between brain iron dynamics and blood-brain barrier function during childhood: a quantitative magnetic resonance imaging study. Fluids Barriers CNS 2023;20:60.
46. Uchida Y, Kan H, Sakurai K, Arai N, Inui S, Kobayashi S, Kato D, Ueki Y, Matsukawa N. Iron leakage owing to blood-brain barrier disruption in small vessel disease

CADASIL. Neurology 2020;95:e1188-98.
47. Langkammer C, Schweser F, Krebs N, Deistung A, Goessler W, Scheurer E, Sommer K, Reishofer G, Yen K, Fazekas F, Ropele S, Reichenbach JR. Quantitative susceptibility mapping (QSM) as a means to measure brain iron? A post mortem validation study. Neuroimage 2012;62:1593-9.
48. Acosta-Cabronero J, Betts MJ, Cardenas-Blanco A, Yang S, Nestor PJ. In Vivo MRI Mapping of Brain Iron Deposition across the Adult Lifespan. J Neurosci 2016;36:364-74.
49. Zheng W, Nichol H, Liu S, Cheng YC, Haacke EM. Measuring iron in the brain using quantitative susceptibility mapping and X-ray fluorescence imaging. Neuroimage 2013;78:68-74.

Cite this article as: Liu X, Hou Z, He Q, Zhao H, Sun S, Hao S, Xie J. Quantitative susceptibility mapping study of deep gray matter iron content in glioma patients. Quant Imaging Med Surg 2025;15(5):4655-4668. doi: 10.21037/qims-2024-2704